SAND REPORT

SAND2005-3307
Unlimited Release
Printed June 2005

Hypervelocity Impact Flash for Missile-Defense Kill Assessment and Engagement Analysis: Experiments on Z

R.J. Lawrence, W.D. Reinhart, L.C. Chhabildas, T.F. Thornhill, D.P. Kelly

Prepared by
Sandia National Laboratories
Albuquerque, New Mexico 87185 and Livermore, California 94550

Sandia is a multiprogram laboratory operated by Sandia Corporation, a Lockheed Martin Company, for the United States Department of Energy under Contract DE-AC04-94AL85000.

Issued by Sandia National Laboratories, operated for the United States Department of Energy by Sandia Corporation.

Available to DOE and DOE contractors from
U.S. Department of Energy
Office of Scientific and Technical Information
P.O. Box 62
Oak Ridge, TN 37831

Telephone: (865)576-8401
Facsimile: (865)576-5728
E-Mail: reports@adonis.osti.gov
Online ordering: http://www.doe.gov/bridge

Available to the public from
U.S. Department of Commerce
National Technical Information Service
5285 Port Royal Rd
Springfield, VA 22161

Telephone: (800)553-6847
Facsimile: (703)605-6900
E-Mail: orders@ntis.fedworld.gov
Online order: http://www.ntis.gov/ordering.htm

SAND2005-3307
Unlimited Release
Printed July 2005

Hypervelocity Impact Flash for Missile-Defense Kill Assessment and Engagement Analysis:

Experiments on Z

R. J. Lawrence, W. D. Reinhart, L. C. Chhabildas, T. F. Thornhill, D. P. Kelly
Sandia National Laboratories
P.O. Box 5800
Albuquerque, NM 87185-1186

Abstract

Kill assessment continues to be a major problem for the nation's missile defense program. A potential approach for addressing this issue involves spectral and temporal analysis of the short-time impact flash that occurs when a kill vehicle intercepts and engages a target missile. This can provide identification of the materials involved in the impact event, which will, in turn, yield the data necessary for target identification, engagement analysis, and kill assessment.

This report describes the first phases of a project under which we are providing laboratory demonstrations of the feasibility and effectiveness of this approach. We are using two major Sandia facilities, the Z-Pinch accelerator, and the two- and three-stage gas guns at the Shock Thermodynamics and Applied Research (STAR) facility. We have looked at the spectral content of impact flash at velocities up to 25 km/s on the Z-Pinch machine to establish the capability for spectroscopy for these types of events, and are looking at similar experiments at velocities from 6 to 11 km/s on the gas guns to demonstrate a similar capability for a variety of research-oriented and applied materials. The present report describes only the work performed on the Z machine.

INTENTIONALLY LEFT BLANK

Acknowledgments

This work was performed at Sandia National Laboratories, Albuquerque, New Mexico. Sandia is a multi-program laboratory operated by Sandia Corporation, a Lockheed Martin Company, for the United States Department of Energy's National Nuclear Security Administration under contract DE-AC04-94AL85000.

Complementary efforts are being supported under a Work-for-Others project for the US Department of Defense, Missile Defense Agency, Corporate Lethality Program, where Marlene Owens has been the supportive program manager.

Additional support from Laboratory Directed Research and Development project 52584 is also gratefully acknowledged. It provided for the initial impact-flash spectroscopy on the Z machine and its analysis, and the resources and expertise to establish a high-speed diagnostic capability for both visible and infrared spectroscopy at the Shock Thermodynamics Applied Research (STAR) facility, which houses our multiple light-gas guns.

A number of the staff at Sandia Labs provided valuable support for the various experiments. For the experiments on the Z machine we thank Marcus Knudson for allowing the initial impact-flash measurements on his magnetically driven flyer shots, and Alan Carlson for setting up and recording the impact-flash spectra on these events. Gregory Dunham provided the calibration and lineouts for the raw spectral data from the Z shots.

INTENTIONALLY LEFT BLANK

Contents

INTENTIONALLY LEFT BLANK

Introduction and Background

The phenomenon of impact flash has been known for many years, even at relatively modest engagement velocities of several kilometers per second. The relevant processes were analyzed in some detail [**1**, **2**, **3**] as long ago as the late sixties and early seventies. More recently impact flash has been proposed as a technique for remote diagnostics associated with the analysis of impact events such as meteoroid impacts on space-based assets [**4**] or even kinetic-energy-based missile-defense kill assessment and target typing.

General Experimental Capabilities and Program Description

We have recently revisited this impact-flash phenomenology by bringing into play our new capabilities for generating hypervelocity impacts at velocities up to several tens of kilometers per second. This particular effort, sponsored by an LDRD from our laboratories, has looked at the flash from impacts over a range of velocities from 6 to 25 km/s, but mainly at the upper end of this range using the Z machine. Additional data at the lower velocities have been obtained on our two- and three-stage light-gas guns, but we will concentrate here on the results of the time-resolved spectroscopy from the highest velocity experiments from Z. Our general goals were to use the measurements of the time- and spectrally-resolved flash output to address three different objectives: 1) data reproducibility; 2) material identification; and 3) temporal evolution of the target.

Specifically, the approximate impact velocity examined was ~25 km/s, with later experiments at ~6 km/s and ~11 km/s. The latter two were accomplished on the light-gas guns, and the higher velocity was achieved using magnetically-driven flyers on our Z machine. Flyer and target materials involved various combinations of aluminum, quartz, and on the gas guns, titanium and indium. Early spectral measurements were in the visible region of the spectrum, ranging in wavelength from 350 to 800 nm, with later results in the infrared, extending from 800 to 1800 nm. For the extremely high velocity shots on the Z machine, which we will be describing here, the outputs from the spectrometers were recorded on streak cameras, and gave time durations for the signal of nearly one-half microsecond. For the gas-gun experiments optical multi-channel analyzers (OMAs) were used, and they gave reading times of almost one millisecond, consisting of up to 200 individual data traces. However, for the latter experiments only about one-tenth of those data contained strong spectral signals related to the impact.

Using standard tabulations of atomic spectral data we were able to identify strong spectral lines from all the principle materials used in the various shots. Using this data we demonstrated that the impact flash spectra were qualitatively reproducible from shot to shot with the same experimental techniques, and anticipating the results from the gas guns, from facility to facility using different approaches and methods. Further, the

signals were unique to the individual materials over the wide range of velocities examined, even though some velocity dependence was observed. Late time spectra, in particular those from the Z machine, evolved into nearly continuum profiles, and offered the opportunity to make estimates of the temperature of the impact-generated materials. Thus all three of our original objectives were accomplished.

Missile-Defense Applications for Impact Flash

One of the major problems for missile-defense systems has always been the ability to assess and analyze the effects of an encounter between a defensive weapon system and an incoming threat object. Without this feedback an intercept has no provision for determining if a second attack is required, *i.e*, an effective "shoot–look–shoot" scenario would have difficulties being implemented. Current missile-defense concepts envision a defensive system that uses a direct impact using a kill vehicle with sufficient kinetic energy to disable the threat. Closing velocities for these engagements will always be high—typically above the sound speeds of the materials involved—and as such they are considered hypervelocities. Because hypervelocity impacts always produce an *impact flash*, it is a reasonable assumption that this radiative signal contains information on the materials and time sequence involved in the interaction. The goal of this particular project is thus to provide proof-of-principle that early-time impact-flash data can be used to analyze a missile-defense engagement event and to provide the required data. Given the impact of a defensive kill vehicle with a threat object, the questions that need to be considered are, did the kill vehicle hit a lightweight object, such as a decoy? Or did it hit a heavy object, such as a warhead? If it was the latter, was the warhead a nuclear weapon? Or was it a different type of threat, such as a chemical or biological weapon? And finally, if it was a weapon, was the device fully disabled or killed? This project addresses these issues by conducting laboratory-scale tests, initially on basic materials but also on applied materials, primarily in our three-stage light-gas gun. However, because we had little experience with flash spectroscopy, our first experiments, which we describe here, were conducted on the Z machine, where spectroscopy is a routine area of expertise.

To give a rough idea of the sequence of events involved in a typical engagement scenario, Figure 1 shows a schematic of a generic kill-vehicle/target interaction, along with some late-time optical data actually taken from an intercept from a missile-defense integrated flight test. Figure 2, which follows, provides a time-resolved plot of the intensity of that optical data. It can be seen that the initial interactions take place on a microsecond time scale, but it takes hundreds of milliseconds for the debris from the collision to disperse from the point of engagement.

To put these various phases of the engagement in a little better perspective, we examined a series of multi-dimensional hydrocode calculations [**5**] of a hypothetical intercept event of about the right physical scale. If the initial impact occurs at zero-time, then the shock-wave and material responses of the outer target layers take place during the first several to roughly ten microseconds. The aeroshell of the target is penetrated at a time, $t \approx 20$ μs.

Most internal components of the target are mechanically loaded by $t \approx 200$ μs. The kill-vehicle and target system is fragmented, and the resulting debris cloud begins to expand by $t \approx 500$ μs. All of these early-time events occur within ~0.5 ms from the initial impact. Thus any temporal information regarding the configuration or structure of the target appears in the radiative output during this limited time. The typical optical data shown above has a time resolution of about 1000 frames per second, or an inter-frame time of one millisecond. Thus all the events related to the detailed configuration of the target occur roughly between the first two frames of this optical imagery. In the intensity plot in Figure 2 this data is all contained in the initial peak; the much broader and later-time signal is mostly the output from the expanding debris cloud. We see that for a full description of all the engagement phenomena, we need early-time, high-resolution measurements, as well as late-time descriptions of the radiative and optical output. Both of these types of data are complementary for describing the entire interaction event.

Note that the two-pulse structure shown in Figure 2 is roughly analogous to that hypothesized in an early description [**1**] of impact flash. In that work it is suggested that the early-time spike can be attributed to the jet that occurs when the impactor first strikes the target, and that the later-time signal arises from the luminous expanding debris cloud. Here the initial spike occurs as a result of the first interactions, and may indeed contain some elements of jetting, but it also contains data associated with the materials and spacing of the layers in both the complex target and kill vehicle. The late-time signals, at many milliseconds, are in all cases identified with the expanding debris.

Because we are making spectral measurements, we should look briefly at the conventional electromagnetic spectrum, as shown in Figure 3. Our impact-flash measurements were made initially in the visible wavelengths, and more recently in the near infrared. In particular our visible data include wavelengths in the range $350 < \lambda < 800$ nm, and our infrared capability extends over the range $800 < \lambda < 1800$ nm. For missile-defense applications, as well as for our laboratory-scale experiments, the early-time radiative signals will be associated with electronic transitions in the atom, and will thus be in the regions we are currently studying. At late times (many milliseconds) the debris will be much cooler, will have undergone some recombination, and will be somewhat "frozen" out. At these times the emission will be typically from molecular vibrations, and at longer infrared wavelengths. At even later times (tens or hundreds of milliseconds) the debris will be cooler yet, and its characteristic spectra will be more in connection with molecular rotations. These emissions tend to be at longer wavelengths and in the terahertz (THz) regime, which extends roughly from $\lambda \approx 30$ μm to $\lambda \approx 3$ mm. There is some interest in considering THz spectroscopy for missile-defense applications because this particular region is less crowded, and lower temperatures are visible. Data in this regime may be easier to interpret, that is if molecular species are present and are cataloged. In fact, we are considering the development of the capability to measure flash output in this spectral regime on our gas guns.

Virtually all operational spectral measurements will be conducted from remote locations, but because of the atmosphere this may be difficult from, for example, the Earth's surface. From the atmospheric transmission plotted in Figure 3, we see that the visible

and near infrared are the most desirable wavelengths for remote sensing. However, most current operational concepts envision a sensor platform associated with the kill-vehicle system, which would function largely in an exo-atmospheric mode. Thus atmospheric transmission may not be a major issue.

Finally, we note the basic overarching objective for this project with regard to missile-defense applications. Given an engagement between a kill vehicle and a threat object, we need to be able to answer the questions mentioned above—did the kill vehicle impact a lightweight decoy-like object, or a heavy object, likely an RV warhead? If it was a warhead, what type of payload did it carry—nuclear, chemical, or biological? Here we are performing laboratory-scale experiments to provide proof-of-principle that impact-flash measurements can be used to provide the required operational answers.

Experimental Effort on the Z Accelerator

The first impact-flash spectroscopy experiments under this project were conducted on the Z machine at Sandia National Laboratories. We had little experience with spectroscopy, and in particular, that due to hypervelocity impact flash. We wanted to leverage the expertise in this area that resided with the staff at Z. The goal was to transfer that diagnostic capability from the Z machine to the light-gas guns at the STAR facility. That transfer of technology turned out to be impractical, but we gained valuable experience at much higher impact velocities than we could have achieved on the gas guns.

Overview of the Z Machine

The Z machine at Sandia National Laboratories typically uses a cylindrical array of very fine tungsten wires to implode on axis to create a region of very high-temperature plasma. This axial convergence is driven by the Z-pinch phenomenon, and generates a plasma that will radiate like a black body at temperatures as high as hundreds of electron volts (1 eV = 11,604 K). This front end is located in the target chamber, which is indicated in the schematic of the machine shown in Figure 4. The inset shows an open-shutter photograph of the electric discharge that occurs during an actual shot, and gives some idea of the large amount of energy that is released. If the high current is shunted through a dead short instead of through the wire array, the same forces can be used to smoothly accelerate metallic flyers to extremely high velocities—approaching 30 km/s or more. They are termed ICE shots for Isentropic Compression Experiments. The concept is that by applying a load to a flyer in a gradual, quasi-isentropic fashion, *vis-à-vis* as a shock wave, the flyer can be accelerated to much higher velocities without the excessive temperature increases associated with shock loading. It is this latter configuration that was used for our impact-flash spectroscopy experiments.

Description of the Z Experiments

The impact-flash spectroscopy shots were actually conducted as ride-along experiments on two of a series of shots conducted by Knudsen [**7**] to study and extend the ability of the Z machine to throw flyers using the ICE approach. The goal of this improved capability is to enable well controlled equation-of-state measurements at ever more extreme conditions.

The target fixture is shown in Figure 5. It illustrates a rectangular configuration with a total of four individual flyer/target pairs, two each on opposing sides. More would be possible (*e.g.*, eight, two on each of four sides), but this four-sample arrangement seems to be ideal for achieving a maximum flyer velocity. In any case, we participated on two

of these shots. Three spectrometers and streak cameras were available, but only two of the three systems obtained adequate data. Thus we were able to look at two of the four samples on both shots. Optical fibers were used to view the impact flash from a lateral position, aligned parallel with the impact interface. The spectral data were recorded on streak cameras via a grating spectrometer. Data were obtained in the visible region of the spectrum, roughly from λ = 400 nm to λ = 750 nm.

Table I lists the shots on which we obtained impact-flash spectra. The complete set of data, as well as the experiments conducted on the gas guns, is described elsewhere [**8**]. Here we will discuss representative examples of those results. First we note that for both shots the impact velocities were over twice as high as those available on the gas-guns. These velocities are greater than typical missile-defense engagements, but they allow us to look at impact-flash spectra over a much broader range of impact conditions than would be possible with the gas guns alone. The table gives the flyer and target thicknesses. The nominal flight distance was in all cases, 4 mm.

When the shot is fired, the tremendous forces necessary to accelerate the flyers to their high velocities, even if the loads are quasi-isentropic, tend to deform the flyers from their initial plate-like configuration into a bowed structure. In addition to measuring the flyer and target velocities, the multiple pins and VISARs (Velocity Interferometer System for Any Reflector) on each target provide initial signals that indicate the degree of bowing. An analysis of that lack of flyer planarity has been provided by Knudson [**7**], who also provided Figure 6, which shows both an x-ray-like construct from the interferometer and pin records and a plot of the arrival times superimposed on a 2-D numerical simulation. This suggests that the first flash signals from the actual impact come from the center of the configuration, where the flyer is moving faster.

All the impact-flash spectroscopy data were recorded as streak-camera photographic images. Figure 7 is one of the better examples that will allow descriptions of the different features that allow both time and wavelength axes to be calibrated and interpreted. The figure is a copy of the raw film image, but clearly shows the many relevant details. To make the time axis specific, we first note that the time fiducial or "impulse" is assigned by the system a time of t = 2686.5 ns. The time calibration or "comb," has a spacing of 4 ns/division. With these references we can fully define the time axis. From interferometer and pin data, also referenced to the impulse, we know that the first impact of the center of the flyer on the target occurs at t = 2740 ns, which we have marked on the figure. The total sweep time for the streak-camera record is approximately 500 ns. With regard to spectral wavelength, two monochromatic lines, λ = 6328 Å and λ = 5434 Å, are written to the film before the shot. (Note that 1 nm = 10 Å.) The first is a characteristic line from a helium-neon laser (HeNe), and the latter is different line, also from a HeNe laser, but shifted toward the green, hence GReNe. The wavelength axis is then fully calibrated by linearly interpolating and extrapolating from these two reference values.

General features of all the data are illustrated in the figure. The various calibration signals are marked with green arrows and the identifications based on those references

are indicated with red arrows. On this particular record we see an absorption line (light colored, $\lambda \approx 5890$ Å) just to the right of the comb, and two prominent emission lines (dark colored, $\lambda \approx 5700$ Å and $\lambda \approx 4500$ Å) somewhat to the left of the comb, and toward the left of the film image, respectively. The absorption line originates from neutral sodium (Na I). The emission line near the comb is from doubly ionized aluminum (Al III), and although less certain, the shorter wavelength emission line is also probably from Al III. To identify these lines the data reduction involves carefully-controlled digital scanning and analysis of the film. The accuracy of the wavelengths thus obtained is about 0.05 percent [**9**], or better than 3 Å or 0.3 nm. To identify the measured wavelengths with specific materials and ionization states we compared the measured wavelengths with those in standard tabulations of atomic spectroscopic data [**10**]. A sample of that data for aluminum is shown in Figure 8.

The film record shows that some of the spectral lines appear before the impact time. We attribute this to vaporized material from the rear of the flyer where the high current is flowing. Because of its very high temperature and pressure, we surmise that a portion of the plasma from this high-pressure region blows around the edge of the flyer, providing early characteristic illumination to the optical fibers.

In addition to identifying spectral lines characteristic of the materials involved in the impacts, we had hoped to determine the temperature of the vaporized and ionized debris generated by the impact. Two regions, as evident in the figure, offer the possibility of continua that might lead to reasonable temperature estimates. The first provides the background to the line spectra and the calibration signals, and the second starts at about 130 ns after the initial impact, and is intense enough to obscure the other signals. Unfortunately, the intensity profiles obtained from these regions cannot be matched with appropriately derived Planckian or black-body curves. We assume that the reason for this is that the density of the debris is quite low, and thus the material is probably optically "thin" and measured radiation does not come from any single region or location that could be considered to be in thermal equilibrium. Further, if the output from the hotter central part of the debris is filtered by cooler lower-density material, its lower energies are more strongly absorbed, and the continuum portions of the profiles would be selectively shifted toward higher energies.

Also the dark region starting at 130 ns after the impact would be consistent with the debris hitting the end of the optical fiber and obscuring further meaningful observation. It is not clear which of these suppositions is responsible for these inconsistencies; it is probably a combination of both. Hence we conclude that even reasonable approximations for the temperature from these probably non-equilibrium conditions are not possible from our spectral data. At this time the best temperature estimates are obtained from numerical [**11**] and analytical [**12**] calculations. The former suggests that the peak temperature at impact is ~7 eV, and the latter estimates that the maximum is ~4 eV, at a pressure of ~7 Mbar, with the aluminum debris dropping to the vicinity of 0.5 eV on release.

Finally, we do not know the origin of, nor do we attach any particular significance to the light horizontal region that appears at a time coincident with the initial impact. We do not see a similar feature in any of the other streak-camera film records.

In the following paragraphs we describe some of the results for each of the successful Z experiments, with a few illustrative plots of the data. The complete set of data is collected elsewhere [**8**].

Shot Z1136/N19. This shot and experiment involved a 25-km/s aluminum flyer impacting a quartz (SiO_2) target. The spectral data are quite sparse, but there are a few lines that can be identified. In Figure 9 we show one of the better spectra, from ~65 ns after impact. From the standard database [**10**] we have matched several lines from neutral, singly, and doubly ionized silicon (Si I, Si II, and Si III) and one from doubly ionized aluminum (Al III), as noted in the figure caption. The sodium absorption line that we have labeled 3 appears in all of the Z spectra and probably represents impurities or other materials (salt?) in the target chamber.

Shot Z1136/N21. This experiment is from the same shot as Z1136/N19 and is similar except that the target is aluminum. Figure 10 illustrates one of several good spectra from this impact. Here there is considerably more spectral data than the previous experiment. The lines called out in the plots are those that were clearly evident in the film record shown in Figure 7. Again we see the calibration signals as well as 10 other emission and absorption lines. Na I (3) is again visible, and Al II (8) and Al III (5 and 9) can be identified. Several of the other lines (6, 11, and 12) are absorption features, and we are not sure of their origin.

Shot Z1144/N19. The second Z shot also used the N19 and N21 spectrometer and camera systems, and had target materials the same as the earlier shot, with the present experiment having a quartz (SiO_2) target. Figure 11 provides one of the spectral lineouts from this experiment. It also includes a scaled version of the spectrum from Figure 9, to provide our first indication of the degree of reproducibility for our spectral measurements for nominally the same conditions but on different shots. We see both wavelength calibrations on both traces (1 and 2). The Na I absorption peak, here labeled 4, is at exactly the same wavelength as in the earlier record. The broad peak labeled 5 and 6 in this figure lines up with the similar one in Figure 9, and can be identified with Si I, Si II, Si III, and Al III. The additional lines at 8 and 9 both appear to be Al III. The smaller peak labeled 7 appears to be O II, an element that was not clearly seen in the earlier quartz impact. Finally, we do not know the origin of the two very small lines at either end of the record (3 and 10). But we do see that that the data from two different shots under virtually the same conditions and employing the same materials lead to very nearly the same measured spectral results, albeit with somewhat different line amplitudes.

Shot Z1144/N21. Even better reproducibility is seen in the comparison between the two aluminum-on-aluminum impacts, as plotted in Figure 12. Virtually all the details, with the exception of a few of the relative line intensities, are the same in both records. We again see the Na I absorption peak (3), and the large peaks at 6 and 9 indicate Al II. 6

may also include an AL III line, as do the signals at 8, 10, and 11. The remaining lines (4, 5, 7, 12, 13, and 14), both absorption and emission, have yet to be identified with materials directly involved in the experiments.

The data from these two shots and four experiments on the Z machine established our capability to take detailed spectral measurements from hypervelocity impact events. We were able to identify most of the observed spectral lines as coming from the materials involved in the interactions, and demonstrated that the data are reproducible from shot to shot. Although we were not able to derive the temperature of the impact-generated materials from the continuum portions of the spectra, we did examine in some detail the processes that would be involved in this type of analysis if the debris clouds were in or at least near states of thermal equilibrium.

Temperature Estimates for the Z Experiments

We had hoped to obtain temperature estimates from the debris generated by the hypervelocity impacts in the experiments conducted on the Z machine. Although we were not successful, the analysis process may be of interest for other similar types of experiments.

The procedure begins with wavelength- (or frequency-) dependent measurements of the radiative output from the impact-generated debris. The basic idea is to compare the continuum portions of these traces with the known shapes of Planckian or black-body curves for various temperatures until a match is found. The black-body curves must first be folded through the independently measured sensitivities or efficiencies of the individual spectral diagnostic systems. It is also assumed that the emissivities of the debris material do not vary appreciably over the range of parameters being considered. The second, and probably the most important requirement, is that the radiating material must be in, or nearly in, thermal equilibrium. Only under these latter conditions will the black-body curves be appropriate and characteristic of those materials. To anticipate our results, it is this last criterion that is likely the principle reason for the inability to apply this technique to the present situation. However, we feel that a brief description of the analysis process would be useful to include. The approach is given in some detail elsewhere [**13**]. Two methods are described—relative and absolute. Even though it is inherently less accurate, we looked only at the former because of its much greater simplicity.

For this analysis we have converted wavelengths into photon energies, using $h\nu$ (eV) = 12398 / λ (Å), because plotting black-body curves as a function of the latter is easier, and more intuitive. We first note that the successful impact-flash experiments on the Z machine used two different spectrometer/camera systems, N19 and N21, which were listed in Table I. The radiation collection efficiencies, η ($h\nu$), for these two systems were provided by Dunham [**9**], and are plotted in Figure 13. For a given black-body temperature, T, the appropriate spectral representation is given by

$$I\,(h\nu) = x^3 / (e^x - 1),$$

where I is the intensity, $x = h\nu/kT$, h is Planck's constant (4.136×10^{-15} eV-s), and k is Boltzmann's constant (8.617×10^{-5} eV/K). In practice the independent variable is $h\nu$—the photon energy—and kT is the desired temperature, both in the same units. For a conventional black-body, the peak intensity occurs at $x = 2.82$, or at a photon energy 2.82 times the source temperature. Multiplying the black-body intensity $I\,(h\nu)$ by the efficiency $\eta\,(h\nu)$ for system N21 at temperatures from 0.25 to 5.0 eV gives the curves shown in Figure 14. The raw black-body intensities for these temperatures peak at photon energies from 0.7 to 14 eV, but here the maxima range only from 1.9 to 2.3 eV, so it is clear that these results are almost completely dominated by the efficiencies. We then take a somewhat different set of black-body temperatures, with a greater range of source temperatures, and plot them in the same manner along with the late time spectral measurements from Z1136/N21/Z9, obtained from another lineout from that shot. The results are shown in Figure 15, where we have plotted the curves as functions of photon energy rather than wavelength. This particular spectrum is for $t \approx 230$ ns after impact, a time by which the data have evolved into a continuum that obscures virtually all of the line structure.

The slopes on the rise times seem to match the data quite nicely, and even the overall shapes appear to be similar to the measured profile. However, their location in photon energy is much lower than the data—well outside the uncertainty associated with either the data or the diagnostic calibration. A similar comparison for an early time, $t \approx 70$ ns after impact, is given in Figure 16. Here the data are from a lineout at an earlier time. The results are virtually the same. The rise time and profile shape are both similar when compared with the continuum portion of the data, but the lateral shift is again greater than the uncertainty of either the data or the calibration. Both of these differences in photon energy for the black-body system-response curves are toward lower energies by ~0.2 eV from the measured spectra. In all cases the intensities are relative and have been adjusted to make the plots easier to interpret.

As stated earlier, our conclusion is that the impact-generated debris is at low density, optically thin, and probably not in thermal equilibrium. Hence its radiative output cannot be expected to be Planckian. If we are viewing the hot debris, near the center of the configuration, through much colder and lower density material, the lower energy radiation would be expected to be absorbed preferentially, thus shifting the continuum portions of the curves to higher energies. The latter is what is observed. A second possibility that may also contribute is that the rapidly expanding debris likely coats the ends of the optical fibers, precluding further meaningful spectral measurement. This obscuration may occur at the time the film record becomes nearly continuous, at ~100 ns before the late-time measurements plotted in Figure 15, or about 130 ns after the flyer first impacts the target.

With the temperature estimates suggested earlier for the debris, that is ~4 eV or maybe higher at the instant of impact, and ~0.5 eV on release, the calculated black-body responses shown in the figures more than cover the range of anticipated temperatures.

However, because of the system response of the spectral diagnostics, it is difficult to differentiate among the various curves. So even if the black-body responses did line up with the continuum portions of the data, it would be difficult to use this approach to provide more than a cursory measure of the debris temperature.

A final interesting observation is that the peaks in the measured continuum data, both at early and late times, are at about the same photon energy, ~2.5 eV. If these maxima have even a very tenuous connection with the debris temperature, it would be inconsistent with the fast cooling that is surely occurring with a rapidly expanding debris cloud. In fact, we can examine all the spectra obtained from these shots—any of them that have a discernable continuum with a maximum, seem to have their peak value near $h\nu \geq 2.5$ eV or $\lambda \leq 5000$ Å. To date we have not found a reasonable explanation for this observation.

Conclusions and Further Work

We have met the objectives set out at the beginning of the project. That is, we have shown that we can take high-resolution spectral- and time-resolved optical data from macro-scale hypervelocity-impact interactions. In particular we have shown that the data is reproducible, that we can identify the materials involved in the impacts from their spectral signatures, and that time resolution allows us to suggest features in the evolution of the debris-generation process. This phenomenology thus becomes a feasible and credible technique for remote diagnostics of dynamic engagements such as meteoroid impacts on space structures or various types of missile-defense engagement scenarios.

In complementary experiments on the gas guns we have successfully implemented high-quality visible and infrared spectroscopy and are considering extending that capability to much longer wavelengths in the terahertz frequency regime. Gas-gun shots completed to date have demonstrated results similar to those achieved with the Z machine, but with a broader range of both basic and applied materials. In addition, the time varying nature of the signals enabled us to correlate differing spectra with multi-layer targets containing different materials in the separate regions. Integrating the resulting traces over wavelength brought those time variations into sharper focus. Analysis and documentation of these latter results are in progress.

Future work will involve extending these results to a much broader range of applied materials, including high explosives and various types of composites, as well as small-scale target configurations that may be of interest from an operational perspective. These extended efforts will be conducted almost exclusively on the gas guns and at impact velocities ranging from ~6 to ~11 km/s. Also we are starting to validate measurements taken under this program with hydrocode calculations and spectral analysis codes so that these modeling and simulation techniques can be extended to complex configurations not amenable to laboratory-scale testing.

References

1. B. Jean and T. L. Rollins, "Radiation from Hypervelocity Impact Generated Plasma," *AIAA Journal*, **8**, 1742-1748 (1970).

2. G. Eichhorn, "Measurements of the light flash produced by high velocity particle impact," *Planet. Space Sci.*, **23**, 1519-1525 (1975).

3. G. Eichhorn, "Analysis of the hypervelocity impact process from impact flash measurements," *Planet. Space Sci.*, **24**, 771-781 (1976).

4. J. A. M. McDonnell, "HVI phenomena: applications to space missions," *Int. J. Impact Eng.*, **23**, 597-619 (1999).

5. R. J. Dukart, Private Communication, Sandia National Laboratories, Albuquerque, NM (2004).

6. K. Rohlfs and T. L. Wilson, *Tools of Radio Astronomy*, Springer-Verlag, New York (2004).

7. M. D. Knudson *et al*., "Near-absolute Hugoniot measurements in aluminum to 500 GPa using a magnetically accelerated flyer plate technique," *J. Appl. Phys.*, **94**(7), 4420-4431 (2003).

8. R. J. Lawrence *et al*., *Hypervelocity Impact Flash for Missile-Defense Kill Assessment and Engagement Analysis*, Sandia National Laboratories, Albuquerque, NM (to be published).

9. G. Dunham, Private Communication, Sandia National Laboratories, Albuquerque, NM (2005).

10. J. Reader and C. H. Corliss, Eds., "NIST Spectroscopic Properties of Atoms and Atomic Ions Database," *NIST Standard Reference Database 38*, National Institute of Standards and Technology, Gaithersburg, MD (1992).

11. R. Lemke, Private Communication, Sandia National Laboratories, Albuquerque, NM (2005).

12. M. D. Knudson, Private Communication, Sandia National Laboratories, Albuquerque, NM (2005).

13. G. Dunham *et al.*, “Diagnostic methods for time-resolved optical spectroscopy of shocked liquid deuterium,” *Rev. Sci. Instrum.*, **75**(4), 928-935 (2004).

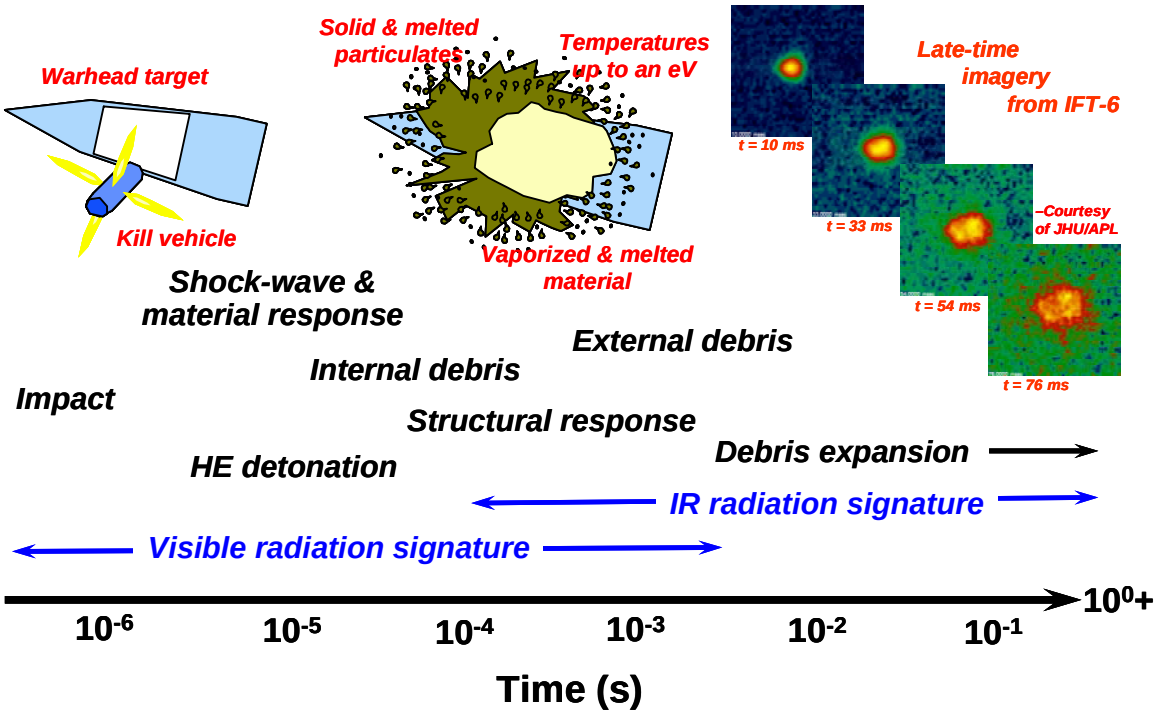

Figure 1. A schematic showing the different phases of a kill-vehicle/warhead engagement. The time scale gives an idea of when the various phases occur, and the approximate spectral regime in which the associated radiative output occurs. Note that as the temperatures cool the visible output tends to give way to the infrared The optical images on the right are from an actual integrated flight test and give a picture of the late-time integrated optical output from such an event.

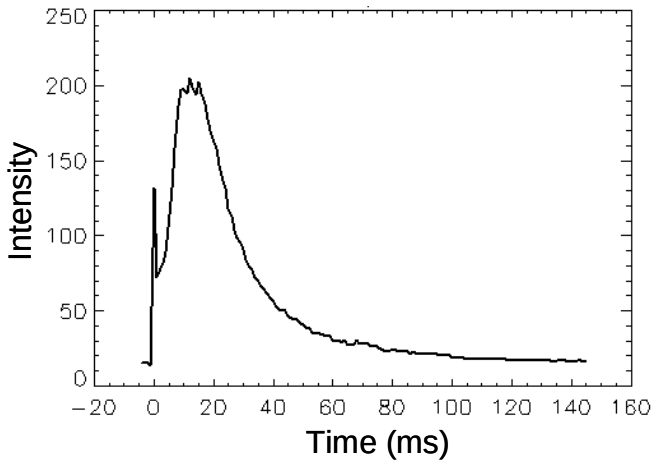

Figure 2. Broad-band intensity from the late-time optical signals of Figure 1. Note that it is the early-time sub-millisecond peak that contains most of the transient data associated with the kill-vehicle/target engagement. (*Courtesy of Applied Physics Laboratory, Johns Hopkins University*)

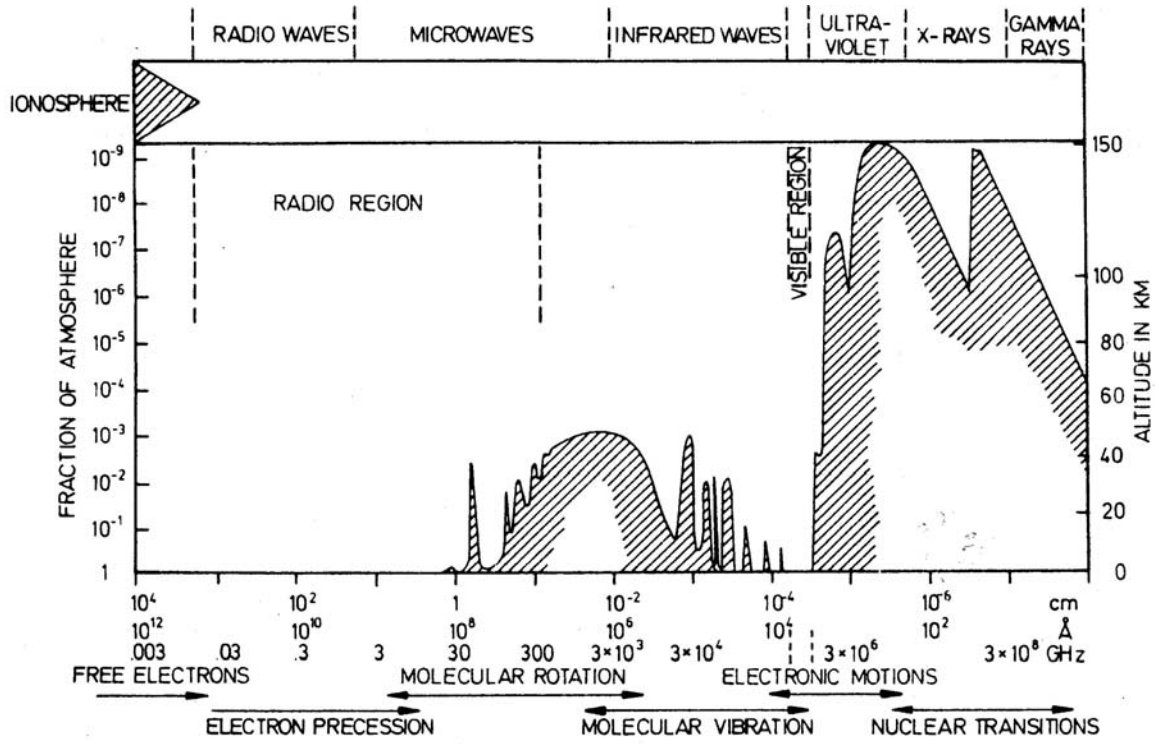

Figure 3. Atmospheric transmission for the electromagnetic spectrum [**6**]. The curve shows the altitude at which an exo-atmospheric source is attenuated by 50 percent. The present work is measuring impact flash spectra in the visible and near infrared. For missile-defense applications there may be interest in extending these or similar measurements to longer wavelengths in the THz frequency regime (*i.e.*, 3 mm > λ > 30 μm).

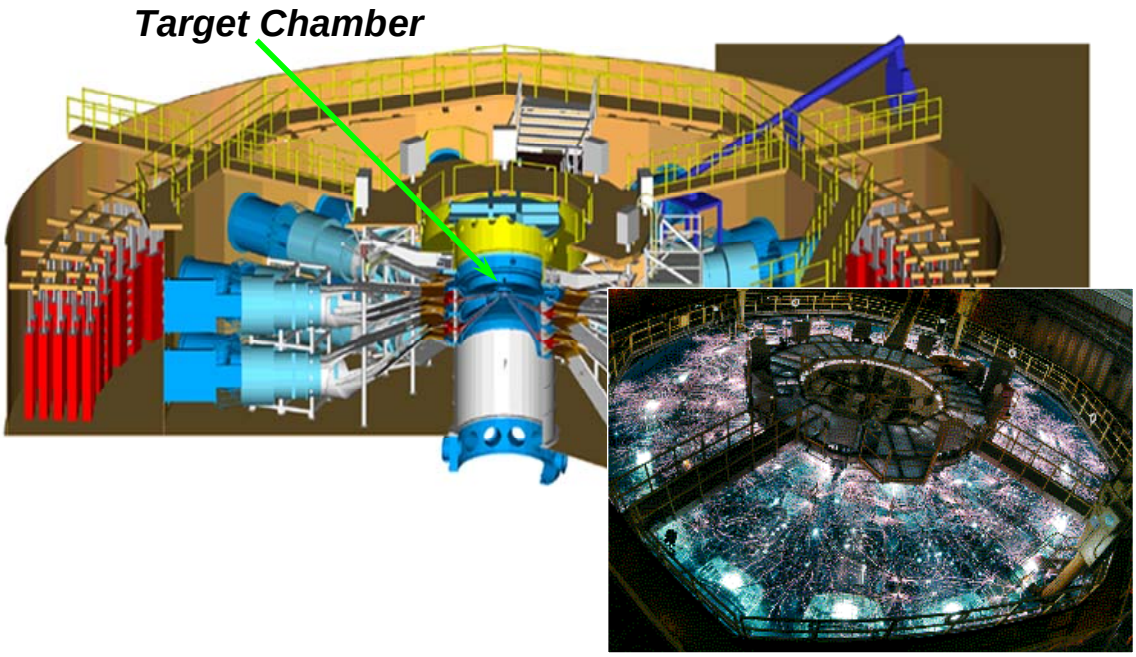

Figure 4. Schematic of the Z machine. The stored energy for Z is ~11.5 MJ, the peak current is ~22 MA, and the rise time is ~200 ns. In a dead-short mode it can throw flyers at velocities up to ~30 km/s. The inset shows an open-shutter photo of the electric discharges that occur when the machine is fired.

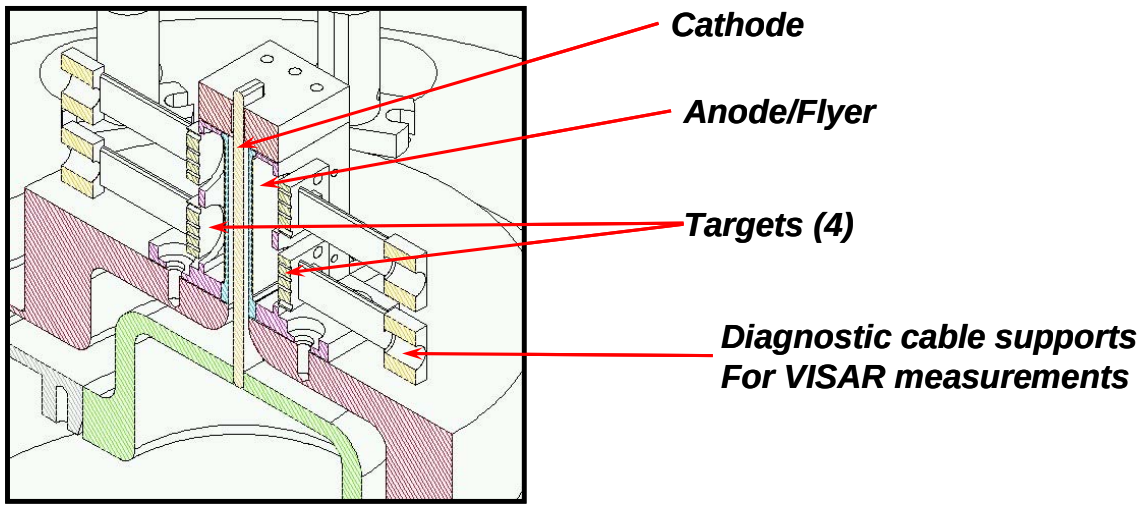

Figure 5. Sample fixture for the hypervelocity flyer experiments on Z. For these shots the fixture is located in the target chamber, which is indicated in Figure 4. The current flows between the cathode and the anode/flyer, and the forces smoothly accelerate the flyer in an outward direction. In this rectangular configuration there are four targets, which are potentially different materials. Each is impacted by the flyer (the anode) of a uniform material. Mechanical signals from the impact are measured from the rear of the target with velocity interferometers (VISARs), and the impact flash signals are measured laterally at the impact interface with fiber optics.

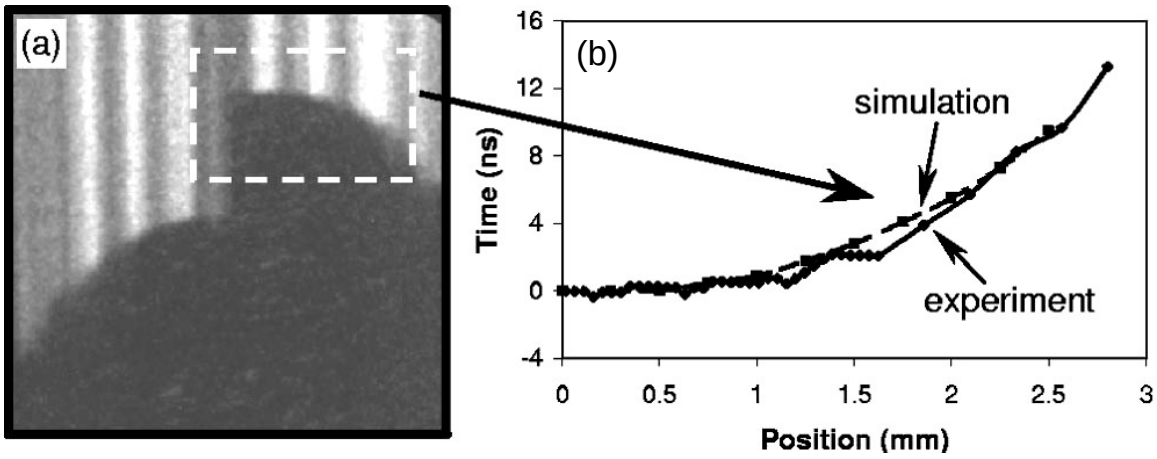

Figure 6. Picture and plot illustrating flyer curvature [7]. An interferometer and pin record showing the actual curvature is in (a), and a plot of the arrival times, along with a 2-D numerical simulation is given in (b). Note that the target is stepped vertically and that only half, from the center out to the edge (the dashed rectangle in (a)), is shown on the right.

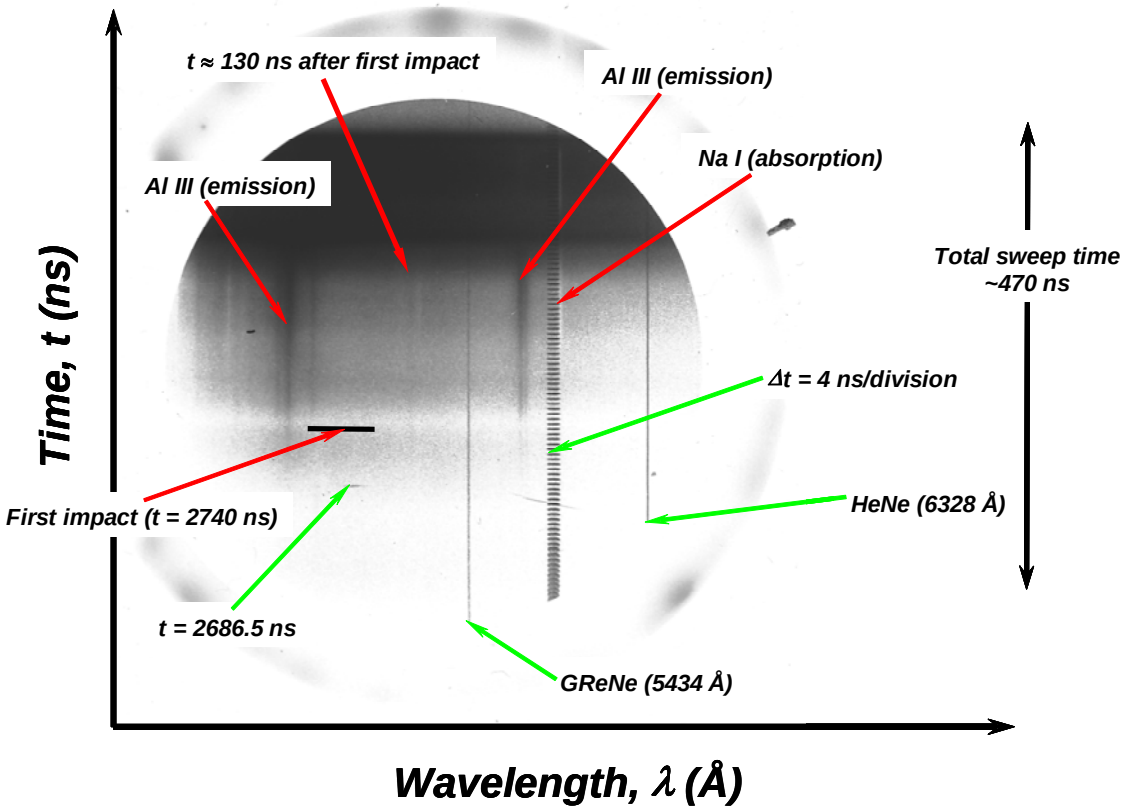

Figure 7. A sample streak camera image from the Z experiments. This one is from shot Z1136/N21, for an aluminum-on-aluminum impact at ~25 km/s. Green arrows indicate calibration signals, both for wavelength and time, and red arrows indicate initial identification based on those calibrations.

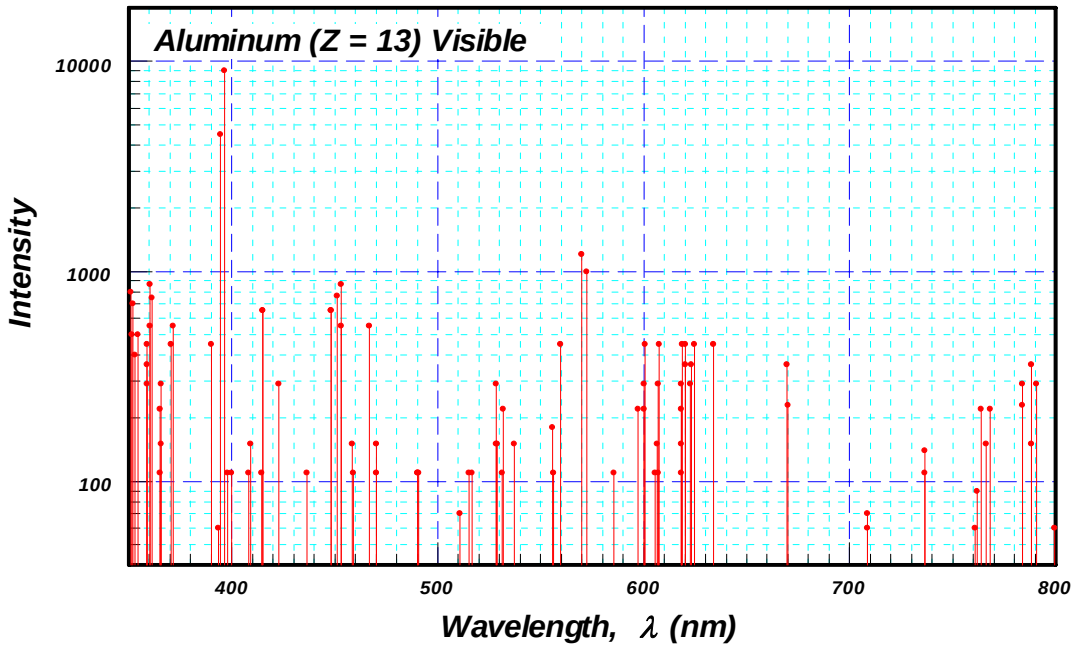

Figure 8(a). Atomic spectrum for aluminum in the visible. This is illustrative of the data contained in the NIST database [**10**], and shows that in this spectral range the line structure can be quite dense.

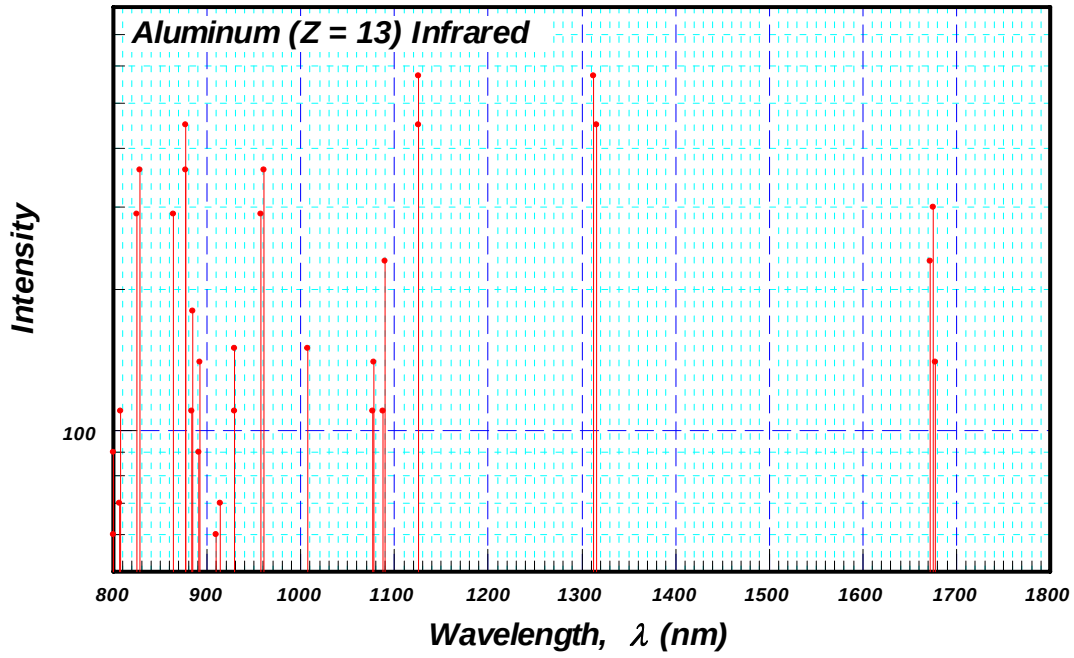

Figure 8(b). Atomic spectral lines for aluminum in the near infrared as contained in the NIST database [**10**]. As with most materials, the atomic line structure is much less crowded in the infrared.

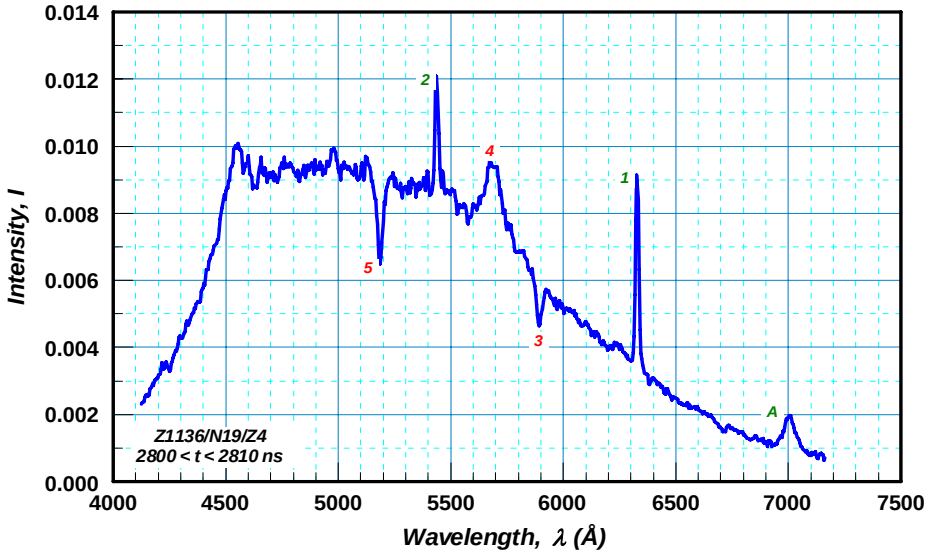

Figure 9. Spectrum from a 25-km/s aluminum impact on quartz. The peaks marked in green (A, 1, and 2) are calibration signals. Those marked in red (3, 4, and 5) represent the measured data. This particular record was taken at a time of ~65 ns after the initial impact. The absorption line labeled 3 matches the wavelength of neutral sodium (Na I), and that labeled 5 has been identified with singly ionized silicon (Si II). The broad peak at 4 appears to contain multiple lines from neutral, singly, and doubly ionized silicon, as well as one from doubly ionized aluminum (Si I, Si II, Si III, and Al III).

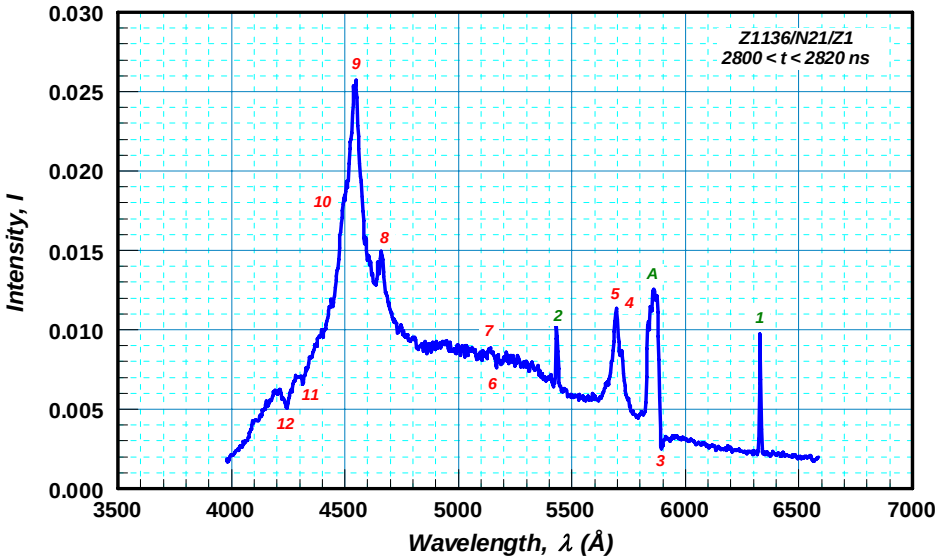

Figure 10. Spectrum from an aluminum-on-aluminum impact at 25 km/s. The peaks with green labels (A, 1, and 2) are calibration signals, and the ones with red labels (3 through 12) indicate the measured data clearly visible in the film record. This spectrum represents a time ~70 ns after impact. As before, 3 identifies an absorption line from Na I, and several of the other lines (5, 8, and 9) can be identified with Al II and Al III.

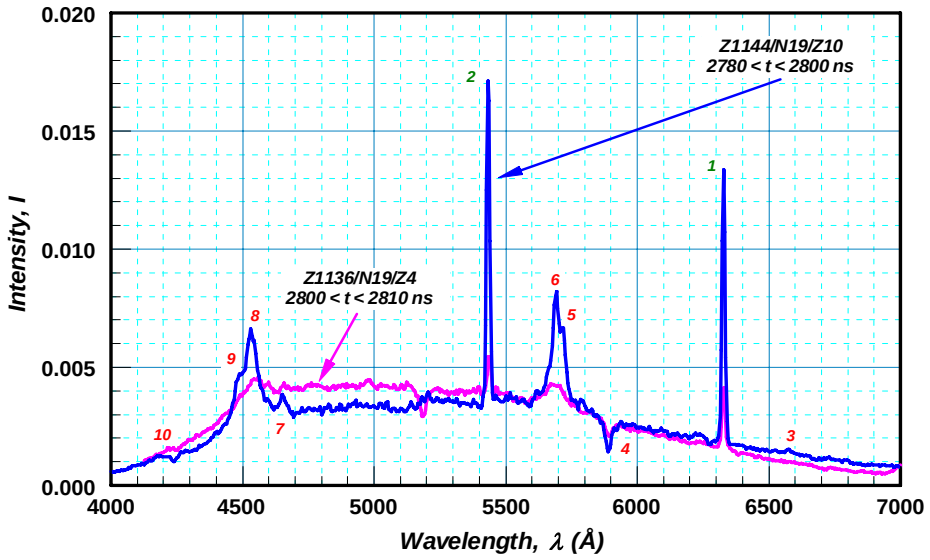

Figure 11. Spectral record from shot Z1144/N19 at a time 90 ns after impact (blue). A scaled spectrum from the earlier aluminum-on-quartz experiment (purple) is superimposed. The labels on the various elements of the line structure are for this figure, and we see that the calibration peaks (1 and 2) line up exactly. Most of the other features, although with somewhat different amplitudes and shapes, also line up well. The one exception to this is the absorption peak at ~5200 Å, which appears in the earlier trace, but not in the present record.

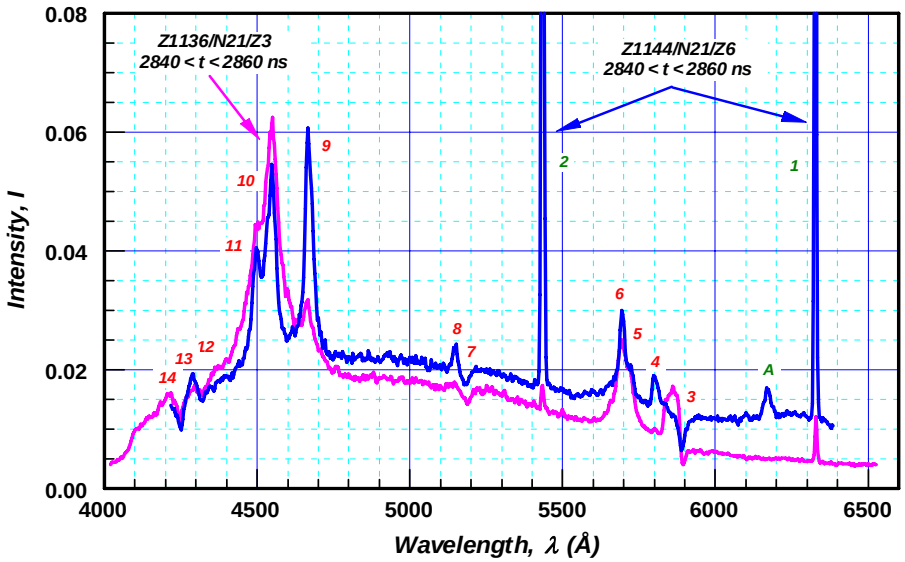

Figure 12. Spectrum from shot Z1144/N21 for aluminum-on-aluminum at 24 km/s at ~150 ns after impact (blue). As in the previous figure we have superimposed a comparable scaled trace (purple) from shot Z1136/N21 to show that in this case the data is reproducible in virtually all its details. Again, for the Z1144 data, the green labels (A, 1, and 2) identify the calibration signals and the red labels (3 through 14) mark the measured spectral lines. The Na I absorption peak (3) is again evident, Al II is represented by 9 and possibly 6, and AL III shows up as 6, 8, and possibly 10 and 11. The remaining lines are uncertain.

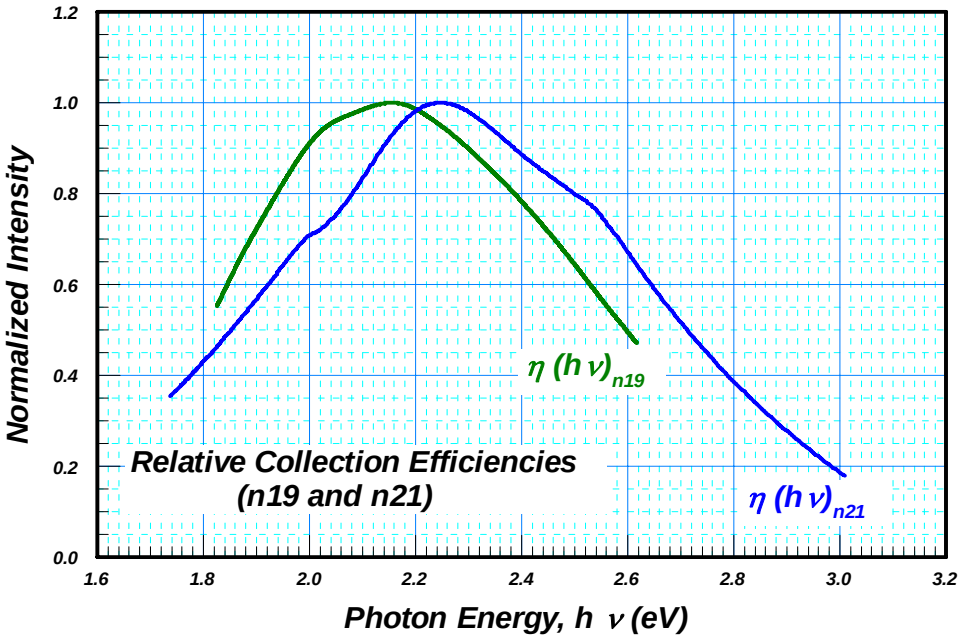

Figure 13. Relative radiation collection efficiencies, η ($h\nu$), for spectrometer/camera systems N19 and N21. These two diagnostic systems were the ones used on the successful impact-flash experiments on the Z machine.

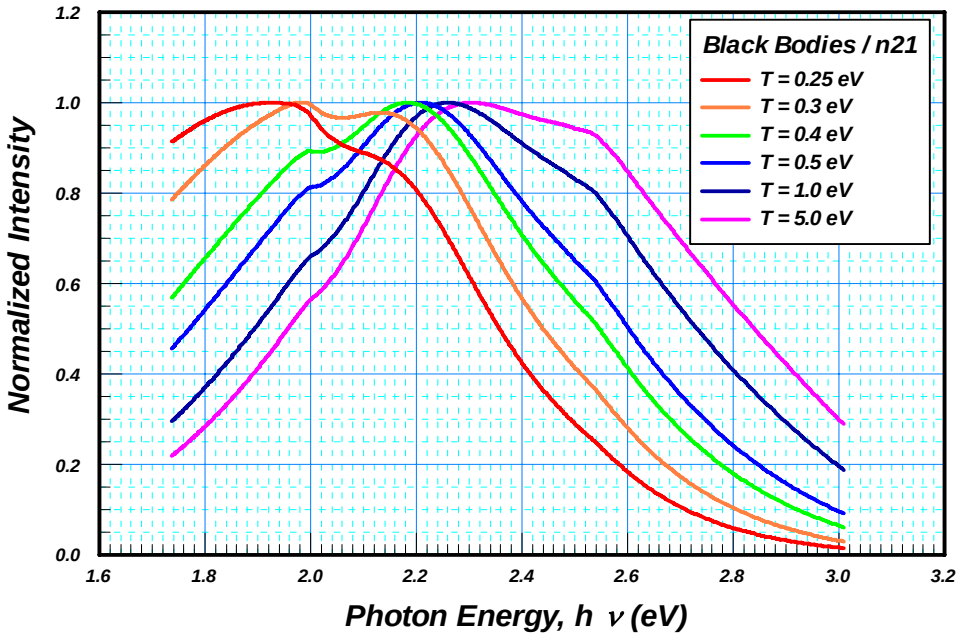

Figure 14. Black-body intensity curves as folded through the efficiency curve for spectrometer/camera system N21. For easier comparison the curves have been normalized to an in intensity of one. Note that the peak intensities vary from 1.9 to 2.3 eV, where the raw black-body curves have peaks from 0.7 to 14 eV. The observed black-body response is thus dominated by the system efficiency.

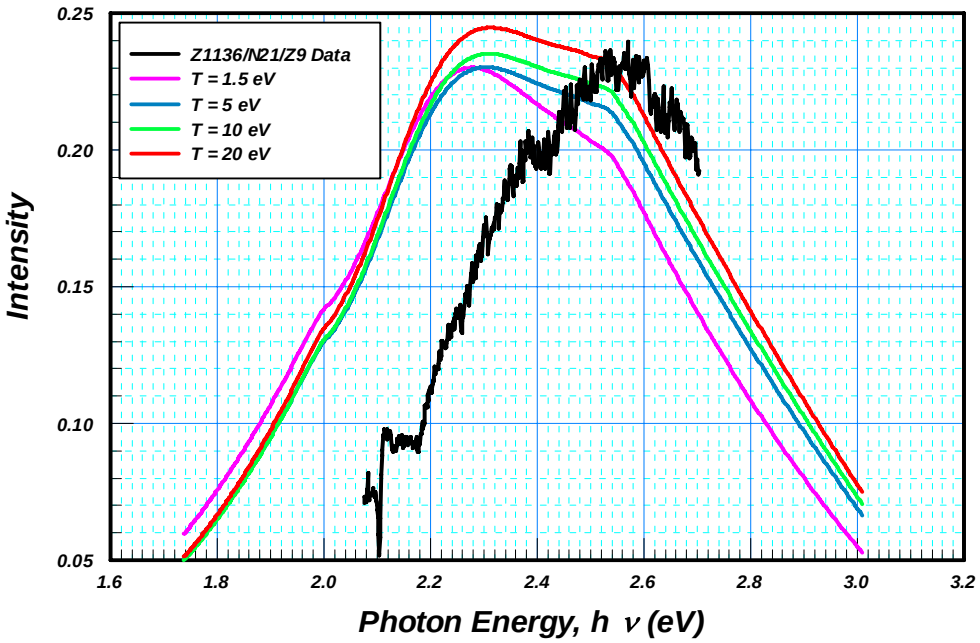

Figure 15. Comparison between late-time data and multiple black-body system responses for a 25 km/s aluminum-on-aluminum impact. The experimental profile is from a late-time lineout using the raw data in Figure 7. The black-body intensities have been adjusted to agree roughly with the experimental data.

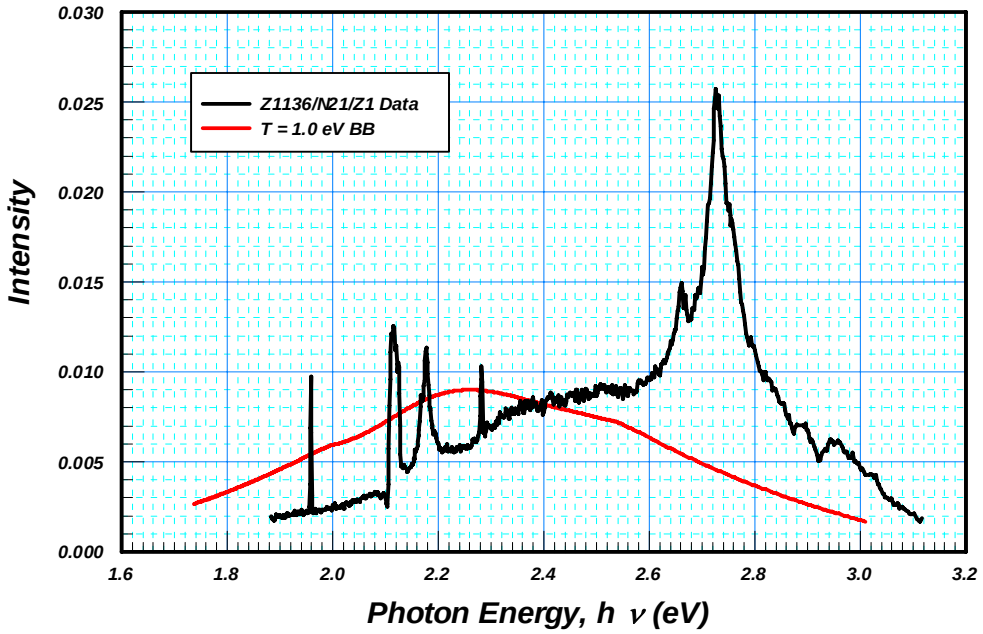

Figure 16. Comparison between early-time data and a 1-eV black-body system response for a 25 km/s aluminum-on-aluminum impact. The experimental spectrum is an early-time record from the raw data shown in Figure 7. The black-body intensity has been scaled to be about the same as the peak of the continuum portion of the data.

Table I. Impact-flash spectroscopy experiments on Z. Three samples were attempted on each of two shots, but only two samples on each shot yielded good data.

Shot Number	*Sample Number*	*Flyer*	*Target*	*Spectral Range*	*Relative Impact Time*
Z1136	**N19**	**0.85-mm Aluminum @ ~25 km/s**	**0.9-mm Quartz**	**400 – 700 nm**	**2740 ns**
	N21		**0.9-mm Aluminum**	**400 – 650 nm**	
Z1144	**N19**	**0.85-mm Aluminum @ ~24 km/s**	**0.9-mm Quartz**	**400 – 700 nm**	**2700 ns**
	N21		**0.9-mm Aluminum**	**400 – 650 nm**	

Distribution

1 MS-0123 LDRD Donna Chavez, 1011
1 MS-1186 R.J. Lawrence, 1674
1 MS-1181 L.C. Chhabildas, 1647
1 MS-1181 T.F. Thornhill, 1647
1 MS-1185 D.P. Kelly, 15417
1 MS-9018 Central Technical Files, 8945-1
2 MS-0899 Technical Library, 9616